An Active Ion Spectrometer for Laser-Driven Ion Beams

Contact: michael.cook@stfc.ac.uk and hamad.ahmed@stfc.ac.uk

M. J. Cook, T. Hall, C. Armstrong, C. Baird, D. Carroll, R. Clarke, J. Green and H. Ahmed
Experimental Science Group, Central Laser Facility, RAL OX11 0QX, United Kingdom

P. Martin, C. Fegan, A. McCay, D. Molloy, O. Cavanagh, S. Kar and M. Borghesi
School of Mathematics and Physics, Queen's University of Belfast, BT71NN, Belfast, United Kingdom

Abstract

We present the development of an active Thomson parabola spectrometer capable of operation at a high repetition rate. The response of different scintillating screens, such as Phosphor screen (P43), glass scintillators (LYSO) and plastic scintillators (EJ260 and BC430), to multi-species ion beams driven by intense lasers, has been studied. Two optical setups, involving direct imaging of the scintillating screen and transporting the light via a fibre bundle, were compared to reveal their efficiencies when transporting light from the detector to the camera. Experimental data showed that Gadox-based Phosphor P43, when compared to other scintillating materials, was the brightest image for a given proton energy, allowing for a more distinguishable detection for other species present in the laser-driven ion beams. The response of P43 was calibrated against a BAS-TR image plate (IP) to determine the absolute particle number for the proton and carbon ion beams produced. The cut-off energy found for the P43 proton trace was 21.9MeV, a value closer to the figure of 22 $\pm$ 1MeV from BAS-TR, making it a potential alternative with an advantage of its capability to operate laser-driven ion beams at rates commensurate with the upcoming Petawatt-class lasers including EPAC.

1 Introduction

The development of high-power laser technology, along with the practise of laser-driven ion acceleration techniques, has provided an efficient and compact way of producing high energy ion beams with energies up to tens of MeV [1]. Thanks to advancements in ultra thin target production, and the discoveries of more efficient ion acceleration mechanisms like radiation pressure acceleration (RPA) [1], proton energies have been recorded to reach as high as 150MeV [2]. The unique properties of laser-driven ion beams has made them suitable candidates for a wide variety of applications [1]. Examples include proton radiography, or high effectiveness at producing large volumes of uniformly heated warm dense matter (WDM) when compared to traditional methods of x-ray heating or shock compression [1, 3]. Laser-driven ions also have potential for use in hadron therapy as they offer a cost-effective and compact method for accelerating ions, making this form of cancer treatment closer to being more widely accessible [4]. Interactions of laser-driven ions with secondary targets can induce various types of nuclear reactions, which can not only diagnose the laser beam properties but also allow for the execution and application of nuclear physics experiments in laser facilities rather than in accelerator or reactor facilities [1]. For many of these applications, the generation of multi-species ion beams, originating from the chemical composition of the target material or impurities in the target's surface [5], is an important characteristic of laser-driven ion beams.

The characterisation and diagnosis of ion beam spectra is crucial to develop an understanding of the underlying mechanisms of laser-driven acceleration methods such as target normal sheath acceleration (TNSA) and RPA [6]. For characterising multi-species ion acceleration from laser-solid interactions, a Thomson Parabola Spectrometer (TPS) [6], a device which can separate ions based on their charge-to-mass ratio and their energy per nucleon, is a common way to characterise multi-species ion beams [5, 7]. Figure 1 describes a typical setup for a TPS system, in which ions are deflected by both magnetic and electric fields, and detected at a displacement from the centre of the detector screen [6]. The displacements of the ions across the x and y axis from the zero deflection plane can be related to their charge-to-mass ratio by

$$x = \frac{Q}{mv^2} E_0 L_{E1} \left(\frac{L_{E1}}{2} + L_{E2} \right) \tag{1}$$

$$y = \frac{Q}{mv^2} B_0 L_{B1} \left(\frac{L_{B1}}{2} + L_{B2} \right) \tag{2}$$

where Q is the charge of the ion, m is the ion mass, v is the speed of the ion along the z axis, B_0 and E_0 are the magnetic and electric field strengths, L_{E1} is the length of the electric field, L_{E2} is the distance between the start of the electric field and the detector, L_{B1} is the length of the magnetic field and L_{B2} is the distance between the start of the magnetic field and the detector [7].

The nature of the detectors used in the TPS can vary, but passive detectors, ones which need to be scanned

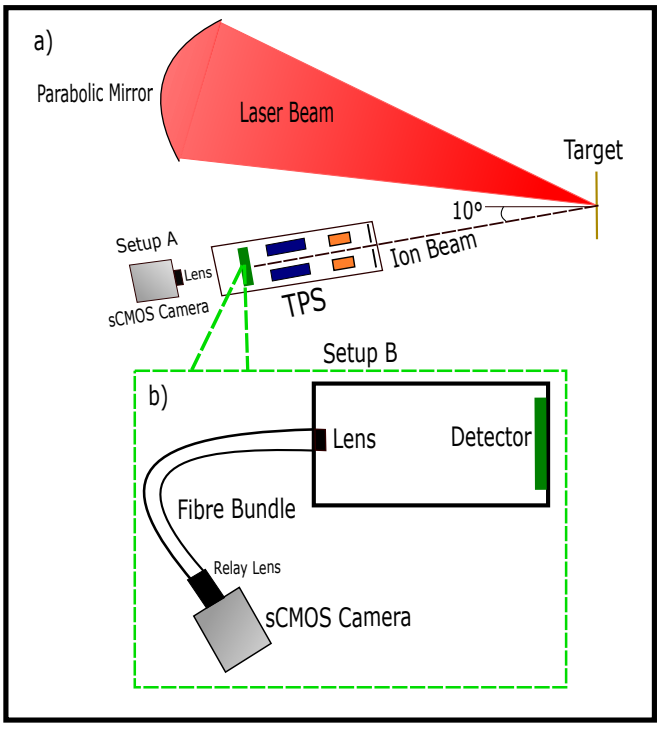

Figure 1: a) Schematic showing a general setup for a TPS device. The ions are deflected by the electric (orange) and magnetic (blue) fields before reaching the detector (green) for characterisation. b) An alternative setup for the Andor Neo Scientific CMOS (sCMOS) camera used in the brightness analysis for scintillating screens. Light emitted from the detector is transferred through a fibre bundle before reaching the camera, rather than projected directly as seen in a).

after each shot to yield the spectra produced by the ion beam, have been a traditional type to use [8]. Examples are image plates (IP), CR39, and radiochromic films (RCFs), but IPs can be favourable due to their reusable aspect (IPs can be wiped after exposure and used again) and high resolution, measuring up to approximately 10μm [9].

Due to the development of high-power lasers capable of operation at 10Hz like EPAC, a problem has arisen where these traditional detectors are difficult to use due to their one time use when characterising ion beams, as well as their need to be scanned to extract information [10]. This scanning requirement means the detector needs to be removed from the target chamber, hence the vacuum within the chamber must be broken between each shot, increasing the time required during experiments [8]. This has motivated the work and development of diagnostics which can accommodate the high shot rates of next-generation high power lasers [8].

Work has been conducted towards active diagnostics, ones which can transfer information live without the need for scanning the detector [8]. Using a CCD or sCMOS camera equipped with an objective outside the vacuum chamber can detect the fluorescence emitted by Micro-channel plates (MCPs) for example [11]. Scintillating materials, both organic and inorganic, have also been suggested, with their high sensitivities and short decay times being able to cope with the increasingly high laser shot rates [10].

Phosphor screens project information similarly to scintillating materials, in which the surface emits photons when incoming particles interact with it, and steadily decays over time [12, 13]. Their efficiency is dependent on structural qualities such as grain size and the thickness of the Phosphor layer, and on certain manufacturing qualities such as the sedimentation of phosphor grains on glass or metal substrates [12, 13]. P43 is one of the types of phosphor screens commonly used in imaging setups due to its high efficiency and spatial resolution from its powder-like composition, but this comes at a cost of a longer decay time [12, 13], a factor which could reduce its effectiveness for lasers operating at frequencies above 1 Hz.

In this article, we report the comparison of sensitivity with regard to the light output from different scintillating materials used as the detector in a TPS, in search for an improved brightness and resolution for high energy ions. P43 scintillating screen produced brighter images in comparison to other scintillators, and was calibrated against a BAS-TR IP to obtain its absolute particle number of the proton beams, increasing the number of detectors which have been successfully calibrated to modern laser systems. We also took two optical camera setups, one which viewed the light emitted from the detector directly, and one which transported the light through a fibre bundle, and compared their image brightness to understand their efficiencies at transporting light from the ion detector material to the camera.

2 Experimental Setup

The data presented in this report was collected from an experiment carried out in Target Area Petawatt (TAP) at the Central Laser Facility, UK [14]. A parabolic mirror focused the beam to a focal spot of $\sim 6\mu$m, corresponding to an intensity of $\sim$ 5 x 10^{20}Wcm^{-2}. For all setups, an Andor Neo 5.5 sCMOS camera was placed outside of the chamber. In addition to shielding over the camera, this protected the camera from strong electromagnetic pulses, reducing the risk of damage to it. The schematics of the setups employed in the experiment are shown in figure 1, which shows the TPS device placed in front of the 15μm thick gold (Au) target at a 10° angle with respect to the target normal. Two optical setups were deployed in the experiment, details of which are given below.

2.1 Setup A: Direct Imaging of P43

The schematic of setup A is shown in figure 1(a), in which the scintillating screen was imaged by a lens that was directly connected to the camera. In this setup only the P43 was employed and calibrated against the BAS-TR image plate to extract the absolute particle numbers of the incident proton beams.

2.2 Setup B: Imaging of Scintillating Screens via a Fibre Bundle

As shown in figure 1b, an image of the scintillating screen was collected by a lens (the same as the one used in setup A) and transported outside of the vacuum chamber by means of a fibre bundle. The image was relayed to the camera by a second lens. The use of a fibre bundle between the camera and lens allowed for reduced light loss, improving image quality, and gave more freedom when it came to the camera's positioning due to the bundle's flexibility [14]. Risks arose however when it came to the fibre being too loose and unshielded, x-ray induced scintillation, and reduced signal to noise ratios [14]. To mitigate this, aluminium and plastic sheets were wrapped around the fibre bundle to reduce the brightness of the background signal being detected [14].

The image brightness from P43 was compared with the other scintillating materials, such as LYSO (glass) [15], BC430 [16], and EJ200 [17] (plastics). TPS parameters, such as pinhole size and the distance of the detector from the magnet, were kept constant to ensure each detector material was under similar conditions and equipment. The size of the pinhole determined the collection of protons in the TPS system, and could therefore influence the brightness of the images. Once images were taken, the stages of the brightness analysis were undertaken as explained in section 3.1. Despite both being acceptable methods at transferring light between the detector and camera, two images, one with setup A and one with setup B, both equipped with the P43 detector, had their brightness for a given ion energy compared to discover which had the most efficient light transfer.

3 Results

The ion beams generated in the intense laser's interaction with the foil targets were characterised by the TPS. Figures 2a & 3a display a raw image of proton and Carbon (C^{6+} and C^{5+}) ion traces accumulated on the P43 screen.

3.1 Brightness Analysis

In order to compare the brightness of the detector materials and the two camera setups, images taken with the sCMOS camera were studied to deduce the counts recorded as the ion traces were characterised. Shown in figure 2a, Python software was used to identify a reference point (the zero point), and plot a vertical lineout at a certain distance from the reference coordinates. The lineout traced was 10 pixels thick, allowing to plot average counts within this width. It was important that the distance between the lineout and the reference point was the same for each image so that each lineout was analyzing the same point, and hence the same ion energy, on the deflected proton beam. Lineouts were traced close to the centre of the proton trace curve to ensure that no counts were recorded from other deflected species present, such as the C^{6+} and C^{5+} ions seen in figure 3a. As can be seen from the graph shown in figure 2b, P43 provided a brighter image than the other scintillators, which can be attributed to its higher density and grain-like structure [12, 13]. Moreover, a thin reflective Al layer on the surface of P43 reflects most of the light emitted from the phosphor towards the sCMOS camera, further improving the detector's efficiency. It can be seen for the scintillating materials that the brightness peaks were rougher and wider compared to the peak produced for P43. This could suggest a lower signal-to-noise ratio, in which the dimmer traces yielded by other scintillators were harder to distinguish from the background noise.

The light output from P43 screens were compared in the setups A and B. Despite their separate resolutions, the lineouts were taken at the same distance from the zero-point. Lineouts were also taken at equal widths to provide an average count for a given point across the y-axis, providing a smoother curve with reduced noise.

While both setups can be deemed an appropriate way of transferring light between the lens and sCMOS camera, figure 2c expressed direct imaging to transfer the most light for a given range of proton energies, making this setup the most suitable method when it comes to experiments in need of high ion sensitivities.

Setup B, involving the connection between the sCMOS camera and lens using a Fibre Bundle, was shown to produce a dimmer image with P43 compared to setup A, which used direct imaging. This supports the risk of the bundle dissipating light where the bundle is loose or unshielded [14]. The brightness peak seen in figure 2c for the Fibre Bundle was much narrower compared to that from direct imaging. This could suggest a much thicker parabola segment from direct imaging, meaning protons were deflected to a greater range of displacements from the y-axis. Both curves were shown to contain noise, especially at lower brightness where the signal-to-noise ratio would be lowest. This can highlight the importance of using detectors of higher sensitivities, ensuring that the image produced is distinguishable against the background light and keeping the signal-to-noise ratio to a minimum. The noise is distinctively higher for the fibre bundle, which could be explained by x-ray scintillation occurring, a phenomenon where electrons interact with the metal connections between the bundle and lens/camera, emitting x-rays and thus increasing the

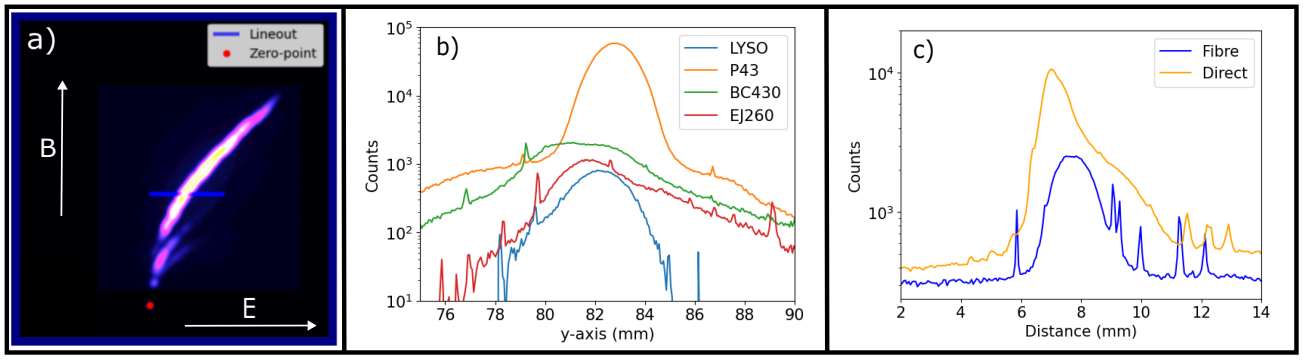

Figure 2: a) Procedure of plotting the vertical lineout across the proton beam at a constant distance from the zero-point. The raw image shown was produced from P43 through a 1mm pinhole diameter. b) Relationship between the image counts (on a log scale) and the distance across the y-axis for different detector materials after performing the lineout procedure. It was clear that P43 produced the brightest image compared to the glass and plastic scintillators, confirming its higher sensitivity to ion beams. c) Comparison between setups A and B for the light transmitted between the lens and sCMOS camera. For a given range of proton energies traced over, it can be seen that direct imaging transferred the most light compared to when using a fibre bundle, suggesting it to be a more suitable method for experiments requiring high ion sensitivities.

quantity of background noise [14]. This would in turn contribute to the reduction in signal-to-noise ratio [14].

3.2 The calibration of P43

In the calibration setup, a BAS-TR with slots of equal width was placed in front of the P43 similar to the setup deployed in the ref [9], where slotted CR-39 was placed in front of BAS-TR. Figure 3b shows the setup of the P43 calibration, where the BAS-TR is stacked against the P43 screen. Figure 3c shows the raw images of P43 and the IP, where the slotted features could clearly be seen. Figure 3d shows the calibration function applied onto the proton trace spectra produced by P43.

Detectors must be calibrated to the ion species they characterise to determine an absolute particle number for a given ion energy in the beam [7]. Recent experiments have begun work on resolving this, calibrating IPs such as BAS-TR on the response to 1-40MeV proton beams [7], 3-300MeV Carbon ions [18] and GeV Gold ions [9].

Figure 3c represents the images taken for the calibration process. The image in c-I shows the result of the phosphor screen, with the dark gaps revealing the gratings of the BAS-TR placed in front of it. The image in c-II was a scan of the IP, in which the black markings revealed the BAS-TR spacings, with the white gaps showing the phosphor screen.

The spectra for the P43 signal and IP scan from figure 3c were plotted together in comparison. To calibrate the P43, it was required to define the energy ranges of the visible signal peaks seen in figure 3c-I. The P43 signal in each defined energy band had to be scaled by a certain calibration factor, one which ensured that they fell in line with the gaps in the IP scan spectrum.

Once these calibration factors were defined for each energy band, the calibration curve from figure 3d could be plotted, showing the calibration factors against energy per unit mass. Two power functions (shown in green in figure 3d) were fitted across the data points, defined by three fitting parameters calculated using a least squares fitting. These fits were formed as

$$\frac{dS}{dN} = \begin{cases} 15.84E^{4.21}, & E \leq 1.4 \text{ MeV} \\ 74.76E^{-0.41}, & E > 1.4 \text{ MeV} \end{cases} \quad (3)$$

where $\frac{dS}{dN}$ was the calibration factor in bit/p$^+$ and E was the energy in MeV. The fitting parameters defined the calibration applied across the P43 spectra produced using Matlab code, allowing the absolute particle number to be found.

The calibration curve shown in figure 3d was used to analyse the proton spectra from the images taken using the P43 scintillating screen. Additionally, the calibration process was repeated for the carbon 6+ ion beam seen just beneath the proton parabola on the P43 traces, improving Phosphor's characterisation capabilities. The proton and carbon ion spectra reconstructed using Matlab code are shown in figure 4, and shows the maximum energy value recorded across the proton spectrum as 21.9MeV. Importantly, this cut-off energy detected on the P43 screen was similar to that of the BAS-TR IP scan (22 ± 1MeV). This benchmarked the detection threshold of P43 against the widely used IP detector in TPS for laser-driven ion beams.

The calibration of the carbon ion beam was more difficult to define, since there were fewer energy bands that could be characterised by the Phosphor screen, hence

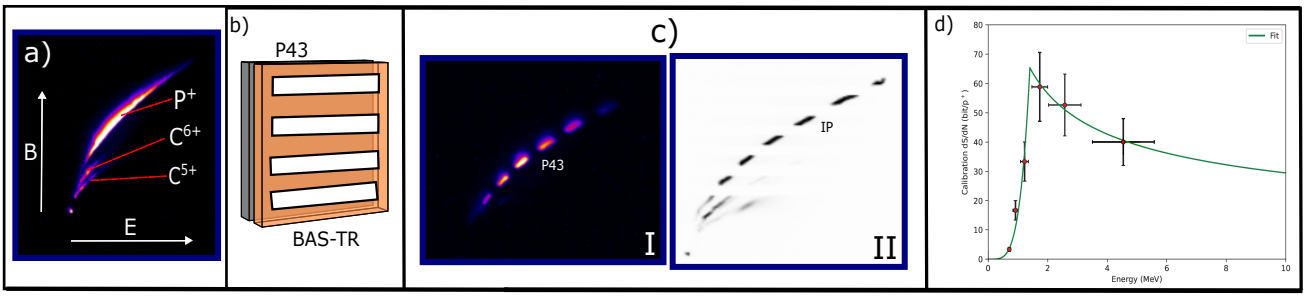

Figure 3: a) Raw image of the ion traces seen when using a P43 detector. The direction of the magnetic (B) and electric (E) fields are shown, and the proton, C^{6+} and C^{5+} ion beams have been successfully distinguished. b) Schematics of the setup used to calibrate P43 scintillating screens against the IP. c) Raw image for P43 (I) with a slotted IP placed in front of it and the image plate scan (II). d) The calibration curve applied over P43 proton trace spectra.

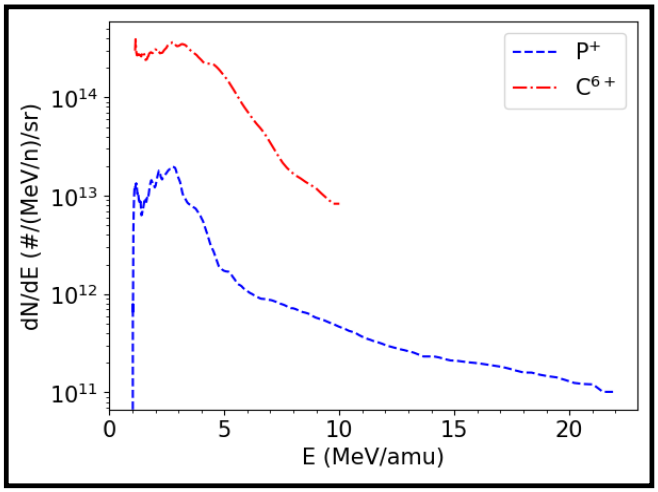

Figure 4: The proton and carbon ion spectra obtained by deploying the calibrated P43 screen. The cut-off energy (the highest E value recorded on the spectrum) for protons was shown to be 21.9MeV, which is similar to that recorded by the BAS-TR IP scan. Due to the scarcity of energy bands characterised by P43, there was a high error for the calibration curve and spectrum defined for the carbon ions, especially for higher energy ranges where no calibration factors could be determined.

there were fewer data points to effectively fit a function to. This large error must be taken into account when applying the calibration to carbon ion spectra, particularly for higher energy ranges where no calibration factors could be defined, and leaves scope for future work where the response functions for heavier ions can be better measured across a wide range of energies.

4 Conclusion

A TPS device was used to investigate the brightness differences between different detector materials and setups, along with the calibration of a phosphor screen. P43 was calibrated against a BAS-TR IP to allow for the absolute particle number for proton and carbon ion traces to be found. The cut-off energy recorded for P43 was commensurate against the well-established IP. Lineout traces revealed P43 to have an overwhelming brightness difference to other scintillating materials, proving P43 to be a strong candidate for a detector requiring high sensitivity and capability of operation at high repetition rates. P46, another type of phosphor screen used in imaging systems, has an efficiency and spatial resolution lower than P43, but has a faster rate of decay, an attractive property for high shot rates [12, 13]. Future studies could compare the sensitivities of different phosphor screens to determine the optimum balance in efficiency, resolution and decay time for high-frequency laser applications. The thickness of the phosphor screen can influence the image brightness; a thickness of about 8-10mg/cm^2 provided optimum brightness with an acceptable spatial resolution when receiving 120keV electrons [19]. Image brightness from Phosphors of the same type but different thicknesses could be compared to determine which is the most efficient for measuring laser-driven ion beams.

References

[1] A. Macchi et al; *Rev. Mod. Phys.* 2013; 85, 751
[2] T. Ziegler et al; *Nat. Phys.*, 2024
[3] P.K. Patel et al; *Phys. Rev. Lett.* 2003; 91, 125004
[4] P. Chaudary et al; *Frontier in Physics*, 2021
[5] A. Alejo et al; *Rev. Sci. Instrum.* 2014; 85 (9): 093303.
[6] D. Gwynne et al; *Rev. Sci. Instrum.* 2014; 85 (3): 033304
[7] P. Martin et al; *Rev. Sci. Instrum.* 2022; 93 (5): 053303.
[8] K. Burdonov et al; *Rev. Sci. Intrum.* 2023; 94 (8): 083303.
[9] D. Doria et al; *Rev. Sci. Instrum.* 2022; 93 (3): 033304.
[10] N.P. Dover et al; *Rev. Sci. Instrum.* 2017; 88 (7): 073304.
[11] A. McIlvenny et al; 2019 JINST 14 C04002
[12] A. Peters et al; *2D-Characterization of Ion Beams using Viewing Screens* 2002.
[13] Proxi Vision, 2023, *Standard P43 Phosphor Screens*, Available from:

https://www.proxivision.de/datasheets/Phosphor-Screen-PR-0056E-03.pdf Accessed: 09/11/2023
[14] D. Bedilu et al; *Deployment of active Thomson spectrometer at Vulcan pettawatt.* CLF Annual Report, 2021
[15] Advatech UK Ltd. 2006 *LYSO(Ce) Scintillator Crystal*, Available from: https://advatech-uk.co.uk/lyso_ce.html Accessed: 12/06/2024
[16] Saint-Gobain Ceramics and Plastics, Inc. 2005 *BC-430*, Available from: https://luxiumsolutions.com/sites/default/files/2021-10/BC430-Data-Sheet.pdf Accessed 04/06/2024
[17] Ejen Technology 2021, *General Purpose EJ-200*, Available from: https://eljentechnology.com/products/plastic-scintillators/ej-200-ej-204-ej-208-ej-212 Accessed 04/06/2024
[18] D. Doria et al; *Rev. Sci. Instrum.* 2015; 86 (12): 123302
[19] A.R. Faruqi et al; 76, 1–2. 1999; 69-75